Journal of Applied Polymer Science

Compatibilization of Polypropylene/Polyamide 6 Blends Using New Synthetic Nanosized Talc Fillers: Morphology, Thermal, and Mechanical Properties

Mohamed Yousfi,[1,2,3] Sebastien Livi,[1,2,3] Angela Dumas,[4,5] Jerome Crépin-Leblond,[6] Mike Greenhill-Hooper,[6] Jannick Duchet-Rumeau[1,2,3]

[1]Université de Lyon, F-69003 Lyon, France
[2]INSA Lyon, F-69621 Villeurbanne, France
[3]CNRS, UMR 5223, Ingénierie des Matériaux Polymères, France
[4]Université de Toulouse, UPS, ERT 1074 Géomatériaux, F-31000 Toulouse, France
[5]CNRS, UMR 5563, GET Géosciences Environnement Toulouse, F-31400 Toulouse, France
[6]Imerys Talc, 2 Place E.-Bouilleres, 31036 Toulouse, France
Correspondence to: M. Yousfi (E-mail: mohamed.yousfi@insa-lyon.fr)

ABSTRACT: New synthetic nanotalc and a commercially available natural fine talc (Luzenac© A3) were chosen in order to establish a comparative study in terms of their contributions on the improvement of the morphology as well as the final properties of PP/PA6 blends prepared by melt processing. At first, the TEM and SEM micrographs showed that both talc particles have a preferential affinity for the more hydrophilic polyamide 6 phase compared with the continuous PP matrix. Moreover, in both cases, the addition of talc fillers induces a significant decrease of the size of the PA6 domains but the better compatibilization efficiency was obtained in the presence of synthetic nanotalc particles. In this work, the positive change induced by the talc nanofillers on the crystallization kinetics and final morphology was highlighted. In addition, compared with natural talc, a highly level of dispersion of talc layers has been obtained with the synthetic nanotalc which is more hydrophilic. Thus, this better dispersion greatly improves the thermal stability of PP/PA6 blends and leads to better mechanical properties (+ 40% in Young's modulus). © 2014 Wiley Periodicals, Inc. J. Appl. Polym. Sci. **2014**, *131*, 40453.

KEYWORDS: blends; thermal properties; morphology

Received 2 December 2013; accepted 15 January 2014
DOI: 10.1002/app.40453

INTRODUCTION

The development of polymer blend based materials has attracted great interest over the past several decades and is currently considered as a very active area of science and technology of great economic importance allowing to synthesize materials with enhanced performances through a low-cost processing. Unfortunately, most of polymers are not miscible. A compatibilizing method is required to achieve satisfactory interfacial adhesion between two immiscible components. Polymer blends are usually prepared by melt processing, and thus the morphological structure of the polymer blends will be governed by different parameters: (i) the shear rate (shear stress) applied to the blend during mixing,[1] (ii) the composition of the blend, (iii) the interfacial tension,[2] (iv) the viscosity ratio (ratio of the viscosity of the dispersed phase to that of the matrix),[3] and (v) the processing parameters such as time of mixing, addition of the compatibilizer, etc.[4]

Typical examples of immiscible polymers are blends of polypropylene (PP) and polyamide (PA6). In fact, they represent two important classes of polymers with complementary properties. For blends containing a PP-rich phase, the polyamide was added because it provides mainly good heat resistance and good tensile properties. However, for PA6-rich blends, the main reasons to mix it with polypropylene have been the need to improve dimensional stability especially in humidity, to reduce water absorption, and to improve impact resistance of polyamide. Research activities concerning the compatibilization of polypropylene and polyamide 6 date back to 1974, when Ide and Hasegawa[5] used maleic anhydride grafted PP (PP-*g*-MA) as a compatibilizer between PP and PA6. However, PP-*g*-MA must be added in a large amount (around 20 wt %) to achieve the desired properties leading to an increase in the price of the final product. More recently, ionomers have been also demonstrated by Willis and Favis[6] to act as compatibilizers between polyolefins and polyamides even with a small amount. The ionomer

Table I. Composition of the Polymer Blends Used

Sample	Designation	m(PP):m(PA6):m(talc) (wt %)
B_0	PP:PA6	80 :20:0
B_1	PP:PA6:A3	80 :16:4
B_2	PP:PA6:HT	80 :16:4

used was (Surlyn® 9020) based on the methacrylic acid functional groups partially neutralized with zinc ions. They concluded that the addition of only 0.5 wt % of the ionomer was sufficient to produce the finest dispersion of the PA6 minor component in the PP matrix due mainly to the strong hydrogen bonding interactions occurring between the ionomer and the polyamide. Also, the mode of addition of the interfacial agent was found to be an important parameter determining the resulting blend morphology.[7]

Unfortunately, the addition of most of the compatibilizers previously used induces a significant loss of blend stiffness. Thus, nanoparticles, especially organically modified clay (organoclay), have then attracted great interest because the nanofiller can play the role of both structural reinforcement and compatibilizer for several types of immiscible polymer blends.[8,9] The use of organoclays as compatibilizers may be suitable for polymer blends with a low processing temperature. Nevertheless, for polymers which require high melt processing temperatures, e.g., polyethylene terephtalate, polyamide and polycarbonate, the degradation of the organic surfactant might lead to a drastic change in the surface energy of the organoclay[10] and a subsequent degradation of the polymer during melt processing which would greatly influence polymer matrix characteristics and would decrease the desired levels of blend properties.[11,12] For overcome these limitations, unmodified solid nanoparticles (without surfactants) such as carbon nanotubes,[13] carbon black,[14] silica,[15,16] and glass,[17] have been used for this purpose. Researchers have proposed several explanations on the compatibilizing effect of the unmodified nanoparticles to immiscible polymer blends depending on the localisation of the filler in the blend. The clay platelets have been located either at the interface,[18,19] in the minor phase[20–23] as well as in the matrix (the continuous phase)[24] or in both components (minor and rich-phase)[25,26] of polymer blends.

In the first configuration, it is now well established that the polymer chains can be physically adsorbed on the clay platelets during melt compounding due to their large specific surface area and act as an effective copolymer which induces a reduction of the interfacial tension.[15] When the clay platelets are dispersed mainly in the continuous phase or in both components, the viscosity ratio between the dispersed phase and continuous one is dramatically changed which can significantly influence the deformability, the breakup of the droplets and therefore the morphological structure of the blend.[3] Recently, some works[27] have investigated the mechanism of compatibilization of immiscible polymer blends by using non-functionalized nanoparticles exclusively located in the minor phase of the blend. The authors studied the influence of T_iO_2 nanofillers on the morphology and crystallization behaviour of PA6 in the 70PS/30PA6 blend. Using TEM analysis, they observed that most of the T_iO_2 nanoparticles were selectively located in the PA6 phase more hydrophilic. The size of the PA6 dispersed domains was decreased upon addition of T_iO_2 nanoparticles. This decrease had a significant effect on the crystallization behaviour of PA6 phase.

In this work, unmodified new nanosized talc fillers were added to act as effective compatibilizers of particular polyolefin/polyamide compounds processed by melt blending. Two kinds of talc were compared an hydrophobic microsized natural talc and an hydrophilic nanosized synthetic one. The role of the surface characteristics of talc has been highlighted. Then, the positive changes induced by the nanotalc on the final morphology, the crystallization kinetics, thermal and mechanical properties of the blends have been detailed throughout in this study.

EXPERIMENTAL

Raw Materials

Polypropylene HP500N (density 0.9 g/cm^3, molecular weight 260 kg/mol, polydispersity index 3.3, melt flow index 12 g/10 min [230°C, 2.16 kg], melting temperature 167°C) was supplied by LyondellBasell (France). Polyamide 6 (PA6) under commercial name Technyl S-27 BL (density 1.13 g/cm^3, melting temperature 222°C, melt flow index 24 g/10 min [230°C, 2.16 kg]) was produced by Rhodia Engineering Plastics (France). The natural talc used (Luzenac A3) with a medium particle size d_{50} of 1.2 μm and a specific surface area of 14 m^2 g^{-1} was supplied by Imerys (France). Synthetic talc was provided by the GET Laboratory (Toulouse University, France).

The abbreviation A3 will be attributed to the natural talc and HT will designate the hydrothermal synthetic talc.

Synthesis of Talc

Nanometric talcs were synthesized at GET Laboratory (University of Paul Sabatier, France) according to a hydrothermal process developed by Le Roux et al.[28] The synthetic talc with a specific surface area of 131 m^2.g^{-1}, corresponding/equivalent to the 6H-talc sample studied by Le Roux et al.,[29] was used as a gel (output of the synthesis reactor).

Processing and Characterization of the Polymer Blends

Blends Preparation. Before extrusion, PA6 pellets were dried in a vacuum oven overnight at 80°C. All polymer blends were prepared using a conical co-rotating twin screw DSM microcompounder at a rotation speed of 240 rpm and the mixture was sheared for about 10 min at 240°C under a nitrogen flow rate of 1.5 bar with and without the presence of talc. All the compositions of the blends are shown in Table I.

For morphology and mechanical characterization, the compounds were injected in a 10 cm^3 mold at 80°C with a laboratory injection molding machine (DSM Xplore 12 ml Microinjection Molder, Nederland) to obtain disk or dumbbell-shaped specimens.

Characterization. Surface energy of natural and synthetic talc was determined with the sessile drop method on a GBX goniometer. From contact angle measurements with water and diiodomethane as test liquids on pressed modified talc disks, polar, and dispersive components of surface energy were determined using the Owens–Wendt theory.[30]

Table II. Total, Polar, and Dispersive Components of the Surface Energy at 20°C on Different Talcs Determined from Contact Angles with Water and Diiodomethane (Measurements on Pressed Talc Powders)

Talc	θ_{water} (°)	θ_{CH2I2} (°)	γ polar (mN/m)	γ dispersive (mN/m)	γ total (mN/m)
HT	34.2 ± 1.4	48.4 ± 1.3	29.6	35.1	64.7
A3	59.7 ± 3.1	42.9 ± 2.3	13.2	38.1	51.3

Thermogravimetric analyses (TGA) of PP/PA6 and PP/PA6/talc were performed on a Q500 thermogravimetric analyzer (TA instruments). The samples were heated from 30 to 700°C at a rate of 20 K min^{-1} under air flow.

X-ray diffraction spectra (XRD) were collected on a Bruker D8 Advance X-ray diffractometer at the H. Longchambon diffractometry center. A bent quartz monochromator was used to select the Cu-Kα radiation ($k = 0.15406$ nm) and run under operating conditions of 45 mA and 33 kV in Bragg–Brentano geometry. The angle range scanned is 1–10° 2θ for the talc and polymer blends.

Transmission electron microscopy (TEM) was carried out at the Technical Center of Microstructures (University of Lyon) on a Phillips CM 120 microscope operating at 80 kV to characterize the distribution of talc particles in the blends. The samples were cut using an ultramicrotome equipped with a diamond knife, to obtain 60-nm thick ultrathin sections. Then, the sections were set on copper grids. ImageJ Software (U.S. National Institutes of Health) was used to estimate the average PA6 domain diameters and their distribution in each sample. A minimum of 200 particles were analyzed for each composition.

The specimens were analyzed by scanning electron microscopy (SEM) on a Phillips XL20 microscope equipped with an energy dispersive spectroscopic (EDS) microanalysis system which used to probe the localization of talc particles in each phase of the binary PP/PA6 polymer blends. For each sample, several (SEM-EDS) images taken at different locations of the sample were collected for statistical analysis. The SEM apparatus was working with a tension of acceleration of 15 KV and a probe current of 130 pA. The specimens were fractured in liquid nitrogen and then coated with gold to avoid charging on the fractured surface prior to the SEM observations.

DSC measurements were carried out by using Q20 (TA instruments) in the range of 10°C to 270°C. The samples were kept for 3 min at 270°C to erase the thermal history before being heated or cooled at a rate of 10 K min^{-1} under nitrogen flow of 50 mL/min. The integration of the exothermic peaks during the non-isothermal crystallization process was carried out to calculate the relative crystallinity as a function of time. The half crystallization time $t^{1/2}$, represents the time needed to achieve 50% of the entire crystallization kinetics.

The crystallinity χ_c (%) of PP and PA6 phases in the blend were calculated by using the following eq. (1):

$$\chi_c(\%) = \frac{\Delta H}{\Delta H^0 \cdot w} \times 100 \quad (1)$$

where ΔH is the specific melting enthalpy of the sample measured in the second heating cycle of DSC experiments, ΔH^0 is the theoretical melting enthalpy of the 100% crystalline polymer matrix (209 J/g for PP[31] and 190 J/g for PA6[32] and w is the weight fraction of PP or PA6 in the blend.

Uniaxial tensile measurements (elongation at break) were taken using a MTS 2/M electromechanical testing system at 22 ± 1°C and 50 ± 5% relative humidity and were performed with a speed of 40 mm min^{-1}. Young's modulus measurements were taken by means of an extensometer using an Instron 4301 machine at a cross-head speed of 1 mm min^{-1}. A minimum of five tensile specimens were tested for each reported value.

The rheological properties were measured in steady shear modes using an ARES rheometer (Rheometrics Scientific) between parallel circular plates with 1 mm gap in a heating chamber. The viscosity was measured at various apparent shear rates increasing from 0.1 to 100 s^{-1} at 240°C.

RESULTS AND DISCUSSION

Surface Energy of Talc Fillers and Polymers

The contact angles and surface energy determined by the sessile drop method on pressed talc powders are summarized in Table II. We can observe that the dispersive component is almost similar but the polar component remains the most variable. As synthetic talc has a larger specific surface area than natural talc A3 one, a higher polar component is obtained (29.6 mN/m instead of 13.2 mN/m). In fact, this difference in polarity can be explained by a overriding presence of hydroxyl groups on the talc layer edges which depends on the specific surface area of nanoparticles. In addition, these values of surface energy determined from contact angle measurements on compressed powders of talc are supported in the literature.[33,34] However, whatever the type of talc used, their surface tension is closer to polyamide 6 matrix one compared with PP matrix one (Table III).

CHARACTERIZATION OF PP/PA6/TALC TERNARY BLENDS

Morphology of PP/PA6/Talc Blends

Scanning Electron Microscopy (SEM) Combined with Energy Dispersive Spectroscopic Microanalysis (EDS). To highlight the affinity of synthetic and natural talc towards the polyamide 6 matrix, the distribution of talc particles has been studied and

Table III. Total, Polar, and Dispersive Components of the Surface Energy at 20°C and 240°C of Polypropylene and Polyamide 6 from Literature

Temperature	Polymer	γ polar (mN/m)	γ dispersive (mN/m)	γ total (mN/m)
20°C	PP[35]	0.4	28.6	29.0
20°C	PA6[36]	29.1	23.8	52.9
240°C	PP[37]	0.3	17.0	17.3
240°C	PA6[37]	9.5	27.7	37.2

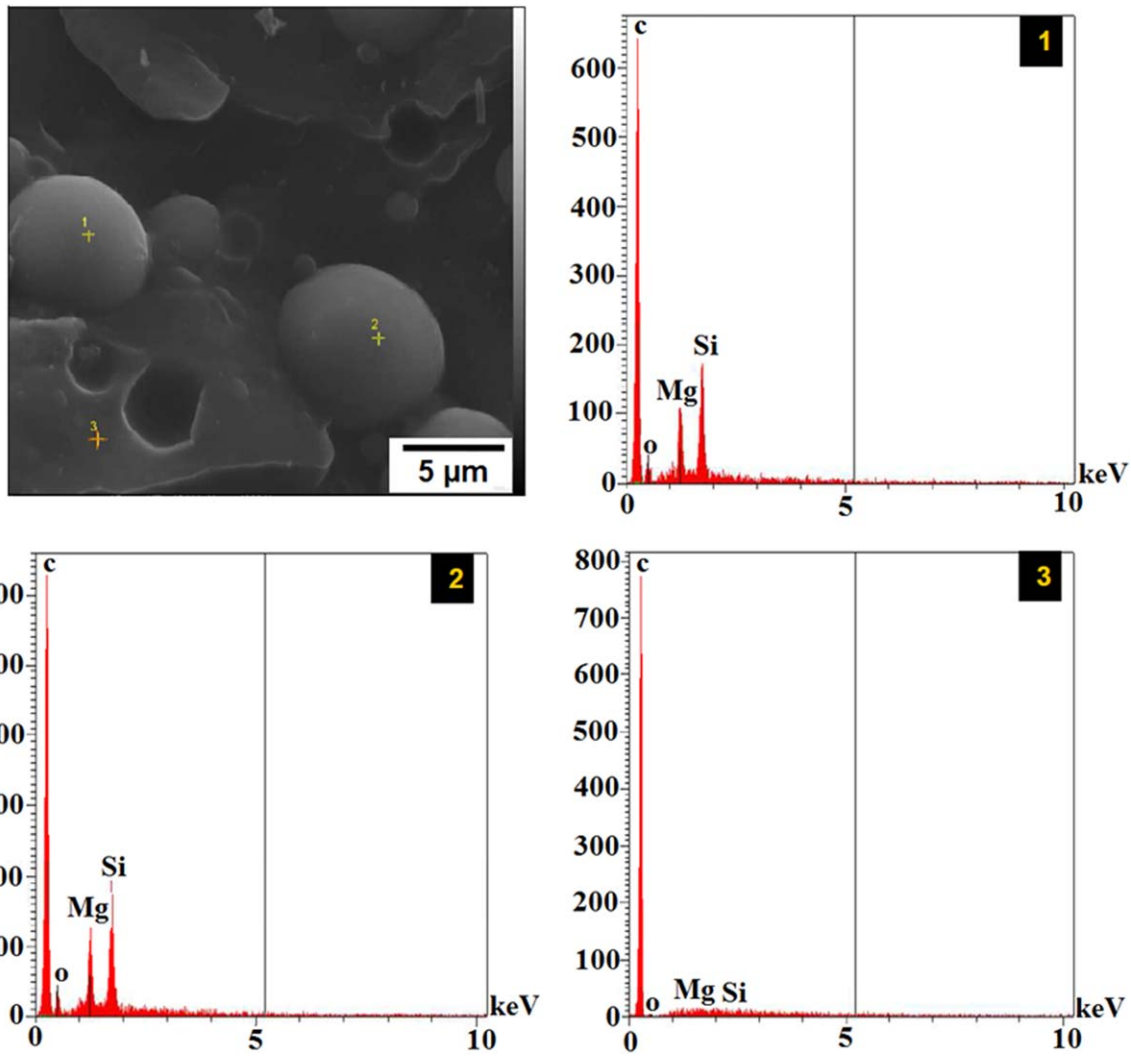

Figure 1. The backscattered electron image of HT talc filled PP/PA6 blends. The Energy dispersive X-ray element analysis spectra (1), (2) of different locations in PA6 domains, and (3) for PP matrix. [Color figure can be viewed in the online issue, which is available at wileyonlinelibrary.com.]

revealed by scanning electron microscopy (SEM) combined to energy dispersive X-ray microanalysis (EDS) in order to determine the exact location of the talc particles in PP/PA6 blends. SEM micrographs carried out on the polymer blends processed with 4 wt % of natural and synthetic talcs are reported in Figures 1 and 2. In addition, the fractured sections were observed perpendicularly to the injection flow (transversal direction). During the fracture process, many domains can pulled away from their previous positions leading to deep holes. In the case of unfilled PP/PA6 blends, large diameters of PA6 domains are observed and the interface was clearly visible, which was typical of poor interfacial bonding.

The backscattered electron (BSE) image of PP/PA6/HT blends shows a contrast between the PA6 domains and the PP matrix which indicates that the talc fillers are most likely located in PA6 phase because talc fillers have a higher atomic number than the polymer. The characteristic peaks of the oxygen, magnesium and silicon characteristics of the talc particles appear only in PA6 phase. In the opposite, the peak of the carbon mainly deriving from the polymer chains as well as the absence of the couple of elements (Mg, Si) in polypropylene matrix suggest that the talc is embedded within the PA6 phase. These results confirm that synthetic talc has a much higher affinity for PA6 phase via strong polar-polar interactions. Indeed, since the PP/PA6 blend components have different surface tensions, hydrophilic talc particles are more inclined to be located in the most polar polymer phase having the higher surface tension (PA6) to minimize the interfacial tension.[22] There are many data concerning this type of solid filler selective adsorption within one phase of the blend which confirms this point of view.[22,23]

Figure 2 shows the backscattered electron image of PP/PA6 blends filled with 4 wt % of natural talc A3. The EDS spectra (1), (2) in different parts of PA6 particles and (3) in PP matrix are presented in Figure 2. As with PP/PA6/HT systems, the natural talc A3 prefers to be located in PA6 nodules instead of the matrix PP. In fact, we found the characteristic elements of talc (Mg, Si) when the cursor is placed in PA6 domains (1), (2) and

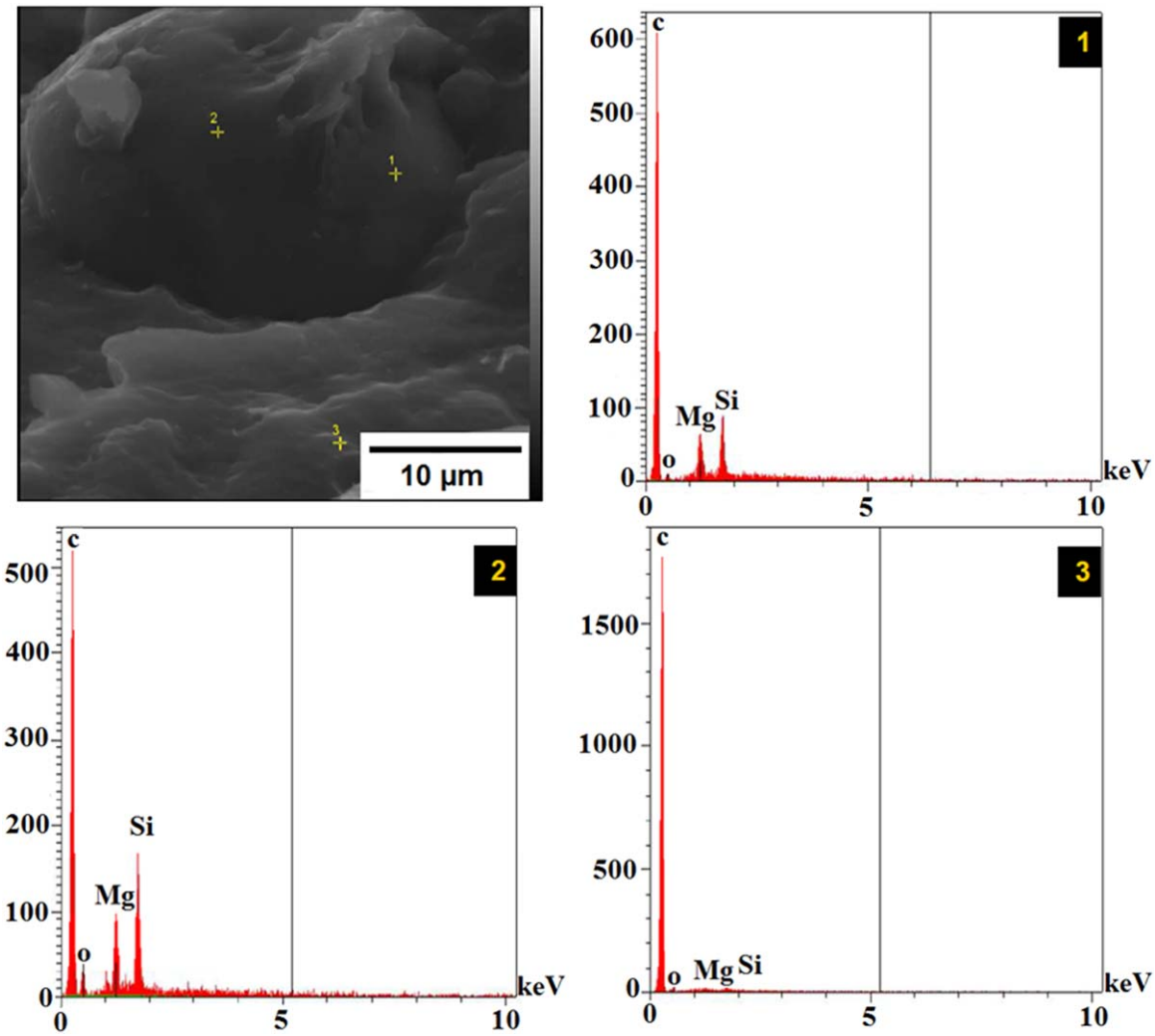

Figure 2. The backscattered electron image of natural talc A3 filled PP/PA6 blends. The Energy dispersive X-ray element analysis spectra (1), (2) of different locations in PA6 nodule, and (3) for PP matrix. [Color figure can be viewed in the online issue, which is available at wileyonlinelibrary.com.]

disappear when it comes to a point in the PP matrix (3). Consequently, the natural talc A3 has an exclusive localization in the minor PA6 phase. This observation has also been proven by Ersoy and Nugay,[22] Gahleitner et al.[23] in similar systems.

In addition, the localization of the talc particles can be predicted also theoretically by the calculation of the wetting coefficient ω_a according to the following equation:[38]

$$\omega_a = \frac{\gamma_{\text{talc-PP}} - \gamma_{\text{talc-PA6}}}{\gamma_{\text{PP-PA6}}} \quad (2)$$

where $\gamma_{\text{talc-PP}}$, $\gamma_{\text{talc-PA6}}$, and $\gamma_{\text{PP–PA6}}$ are the interfacial energies between talc and PP matrix, between talc and PA6 and between PP and PA6, respectively. The values of the different interfacial energies at 240°C were calculated from the values of surface energy (Tables II and III) using the equation of Good-Girifalco:[35]

$$\gamma_{12} = \gamma_1 + \gamma_2 - 2\sqrt{\gamma_1^d \gamma_2^d} - 2\sqrt{\gamma_1^p \gamma_2^p} \quad (3)$$

If $-1 < \omega_a < 1$, the talc will be localized at the interface between the matrix and the dispersed phase. Otherwise, the talc will be preferentially localized in PA6 phase when $\omega_a > 1$. In conclusion, the wetting coefficient values of natural talc A3 and synthetic talc HT were 1.63 and 2.74, respectively. Based on these values and on the SEM micrographs, the natural and synthetic talc would be localized inside the PA6 phase. On the other hand, it has been found that the migration of particles from the incorporated phase in the early stages of mixing toward their preferred phase is easier when the preferred domains are less viscous.[7] In our case, the melt flow index at 230°C of pure PA6 was higher than that of PP. Therefore, nanotalc could easily disperse in the PA6 phase than in the PP matrix.

SEM and TEM Analysis. In order to probe at a nanometric scale the different morphologies of the ternary blends, the distribution and the dispersion of PA6 domains but also of the talc particles in polypropylene/polyamide 6 blends, Scanning and transmission electronic microscopy on the PP/PA6 blend (without talc) and PP/PA6 filled with natural and synthetic talc have been analysed. SEM micrographs are presented in Figure 3 and TEM micrographs are reported in Figure 4 where the dark ellipsoid regions correspond to PA6 domains.

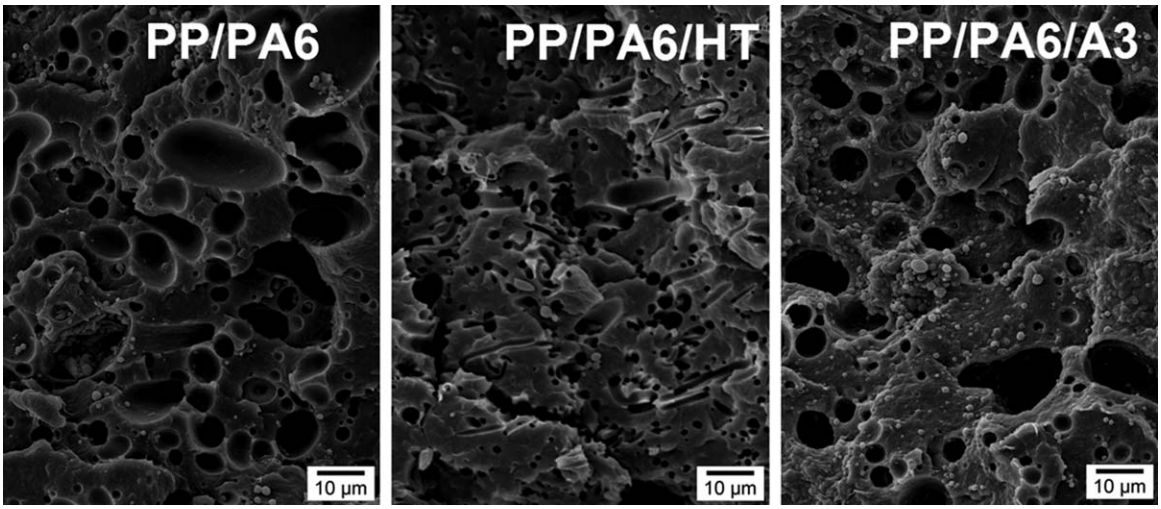

Figure 3. SEM micrographs of the unfilled and talc filled PP/PA6 blends.

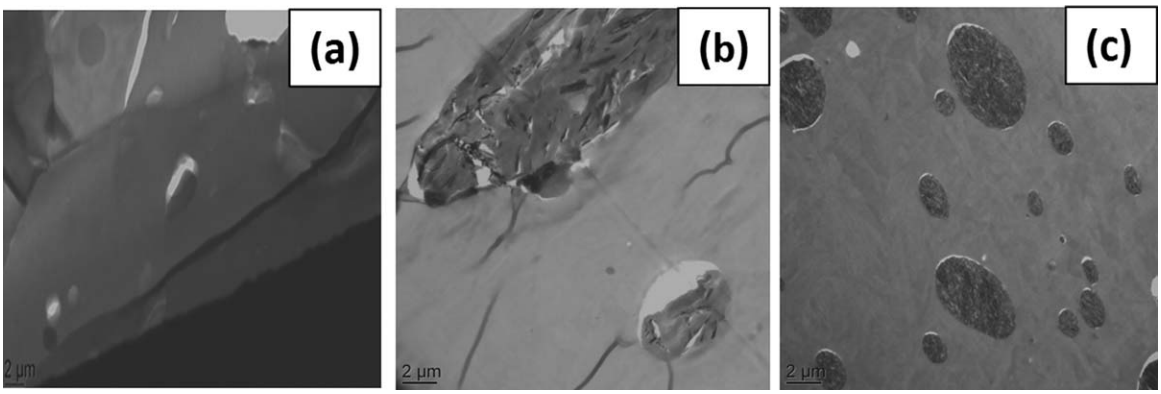

Figure 4. TEM micrographs of the unfilled and talc filled PP/PA6 blends: (a) PP/PA6, (b) PP/PA6/A3, and (c) PP/PA6/HT.

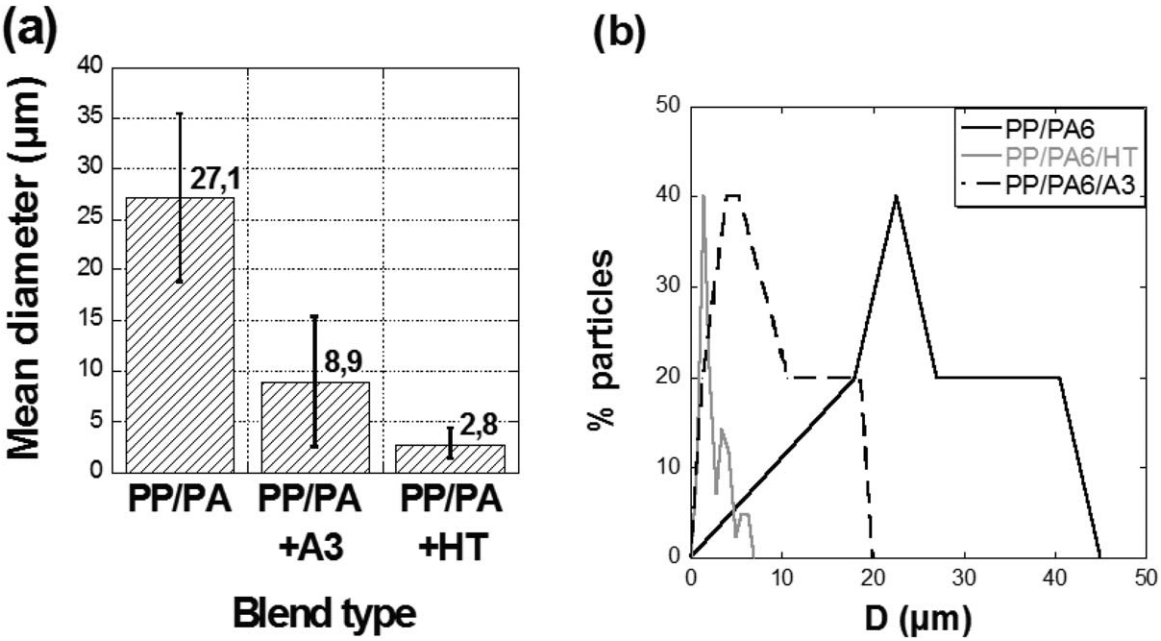

Figure 5. (a) Mean diameter and (b) size distribution of PA6 nodules obtained for the blends using ImageJ software.

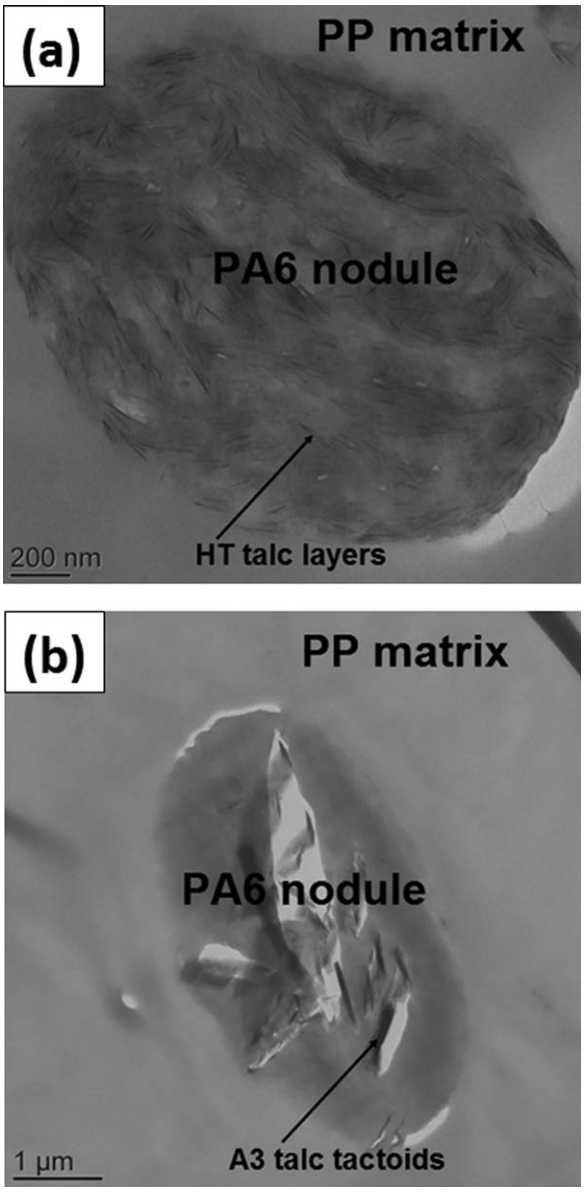

Figure 6. Magnification image illustrating the distribution of the a) synthetic talc HT and b) natural talc A3 inside the PA6 nodule in continuous PP matrix.

In the case of PP/PA6 blends without talc, large domains of PA6 have been observed and calculated by image analysis (diameter $D = 27.1$ μm in average). In addition, the existence of a clear interphase is typical of morphology with a poor interfacial bonding.

In contrast, the addition of talc induces a significant change in the size and the shape of PA6 domains, particularly in the presence of synthetic talc. Indeed, the change of morphology indicates that the compatibility of PP and PA6 is greatly improved in the presence of talc. Synthetic talc (HT) leads to the highest decrease of the PA6 nodules size ($D = 2.8$ μm in average) and the better size homogeneity [Figures 4(b) and 5], whereas A3 is slightly less efficient with a domain diameter of 8.9 μm in average [Figures 4(c) and 5].

Figure 6 shows the TEM images of PP/PA6/HT and PP/PA6/A3 blends at high magnification. Dark lines were assigned to the talc where individual nanosized plates are randomly distributed and oriented in the PA6 nodule [Figure 6(a)] or present under tactoid form inside the PA6 phase [Figure 6(b)]. It is useful to mention that the nanotalc HT used in this study has not undergone any chemical treatment before compounding (unmodified particles). Generally, in the case of montmorillonite (MMT), a surface treatment is required to achieve a similar dispersion in the same polymer.

The decrease of the PA6 domain size upon the talc addition can be explained as follows: (i) in the case of natural talc A3 which is exclusively localized in the dispersed phase in the form of small aggregates, a novel mechanism of compatibilization denoted "Cutting effect" was proposed by Zhu et al.[36] [Figure 7]. During the first stage, when compounded with the immiscible PP/PA6 blends, the talc platelets spontaneously are confined in the dispersed domains due to the low viscosity of PA6 phase, as shown in Figure 7(a). Since the level of interactions between natural talc fillers and polyamide is not strong enough (due to their polarity differences), talc platelets will link together through electrostatic interactions. In order to contain more talc platelets, the fillers in PA6 domains aggregate together and form a special "knife-like" structure. Therefore, the PA6 droplets are torn up along the "clay knife" as shown in Figure 7(b). With further growing, the "clay knife" is strong enough to completely "split" the dispersed PA6 domains apart, and the morphology evolution develops as shown in Figure 7(c). In this stage, more dispersed PA6 droplets are broken up, leading to the reduction of the domain size. (ii) In presence of synthetic talc, another mechanism is suggested to explain the compatibilization induced by the high delamination of nanotalc in the polyamide phase based on the encapsulation of PA6 domains in a three-dimensional network of nanoparticles as mentioned by Cai et al.[37] and Ou et al.[40] in the case of T_iO_2 filled PS/PA6 and PP/PA6 blends respectively (Figure 8). They found that in all cases, T_iO_2 nanoparticles were preferentially located inside PA6 nodules. When T_iO_2 nanofillers were poorly dispersed in the PP/PA6 blends, the dispersed PA6 phase particles are large and irregularly shaped. However, the shape of the dispersed PA6 domains are became regular and a finer morphology was obtained in the case of functionalized T_iO_2 that are more hydrophilic nanofillers. Elias et al.[7,41] found similar trends in the case of nanosilica filled PP (80)/ EVA (20) blends. Compared with the hydrophobic nanosilica, the hydrophilic one has more affinity with EVA minor phase and the final morphology was the most thermodynamically stable one. Thus, when the nanoparticles are well distributed inside the dispersed phase, they can form a three-dimensional network and the droplets will be trapped in the array of nanoparticles. The mechanical stability of the network formed reduces the rate of coalescence leading to a significant reduction of the dispersed domain size.[39] To verify this assumption, the rheological measurements (steady state viscosity–shear rate curves) of PP, PA6 matrix and PA6/HT nanocomposites are performed (Figure 9). It seems that the addition of synthetic nanotalc (4 wt % of HT) induces a significant increase in the viscosity of PA matrix. At a shear

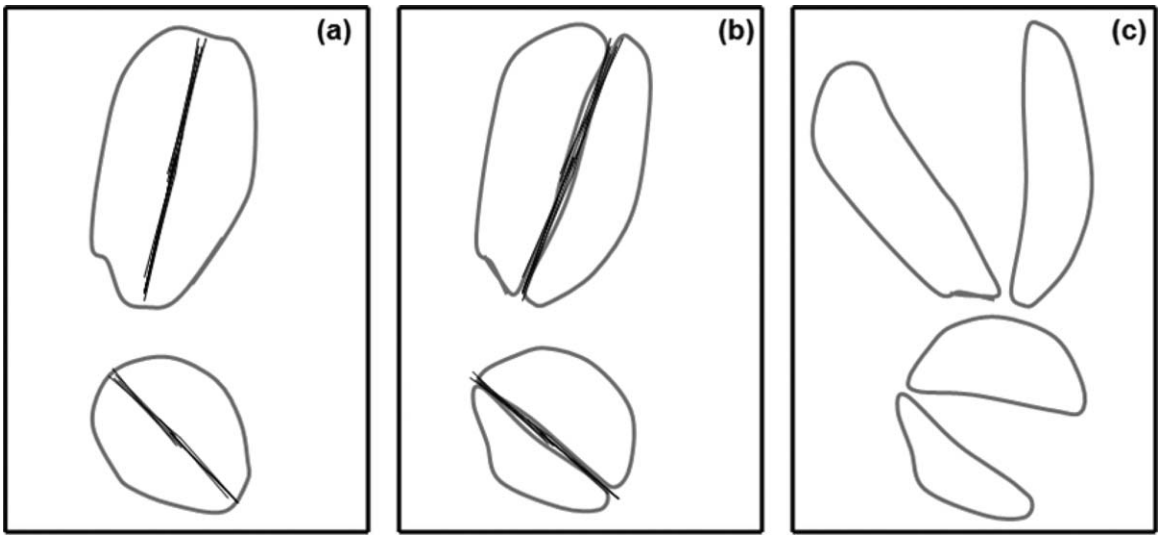

Figure 7. (a)–(c) showing the compatibilization mechanism of clay in immiscible polymer blends according to Zhu's mechanism.[39] Clay tactoids acts like a "knife" thereby reducing dispersed domain size due to shear stress generated during mixing.

rate of 1 s^{-1}, the viscosity of PP matrix was 580 Pa s and for polyamide matrix the viscosity increased from 113 Pa s in the case of unfilled PA6 to 235 Pa s for PA6/HT blends. This increase of the viscosity in the presence of talc platelets would be even greater if the concentration of talc is more important. Note also that the presence of talc not affect the interfacial tension since it does not contain chemical compatibilizer (untreated particles). According to Wu's theory,[42] the smallest dispersed domains are obtained when the viscosity ratio ((η(droplet)/η(matrix)) is about unity. As the viscosity ratio decreases below unity, the dispersed particles become larger. However, in our case, the incorporation of synthetic nanotalc induces an increase of the viscosity ratio (η(PA6/HT)/ηPP) but still below unity. This can support the above-mentioned mechanism and the decrease in the size of PA6 dispersed particles. Si et al.[43] reveal that the size and aspect ratio of solid fillers play also a major role in the stability of the morphology in melt mixed multiphase polymer blends. They proved that high aspect ratio objects are more efficient in reducing the dispersed domain size as compared with low aspect ratio fillers. Indeed, the compatibilizing effect is dependent on the surface area of the filler and its ability to disperse in the polymer melt. The presence of tactoids greatly reduces the interface contact and wetting between the platelets and polymer chains which induces a less stabilization effect.

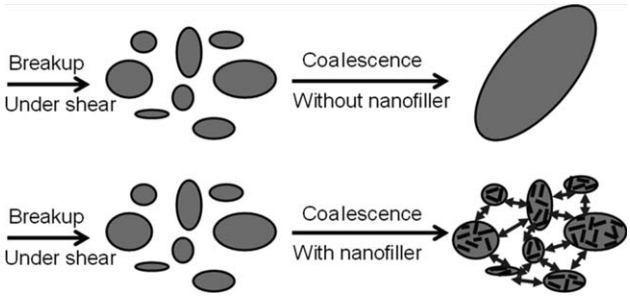

Figure 8. Compatibilization mechanism induced by nanoscale exfoliated talc fillers in the dispersed phase of PP/PA6 blends. The arrows among particles show the ability of droplets to oppose to coalescence.

Structural Analysis of Talc and PP/PA6/Talc Blends by XRD

As TEM provides only a local view of the dispersion state of talc in PP/PA6 blends, further analysis using X-ray diffraction providing bulk data have been carried out. In fact, according to the literature, when the peaks disappear below 10° 2θ, the exfoliation of fillers in the polymer blends is proven. X-ray diffraction patterns of raw synthetic and natural talc and the corresponding PA6/talc or PP/PA6/talc composites are summarized in Figure 10(a,b).

The shape of the XRD curves of the ternary PP/PA6/HT and PP/PA6/A3 blends was very similar to the XRD curves of their corresponding PA6/talc samples, which implies that the dispersion mode of talc particles in PP/PA6 blends was governed by the strong interactions between talc and PA6 phase.

Concerning the PP/PA6/HT blends, the disappearance of the characteristic peak (at $2\theta = 9.1°$) suggests the exfoliation of the

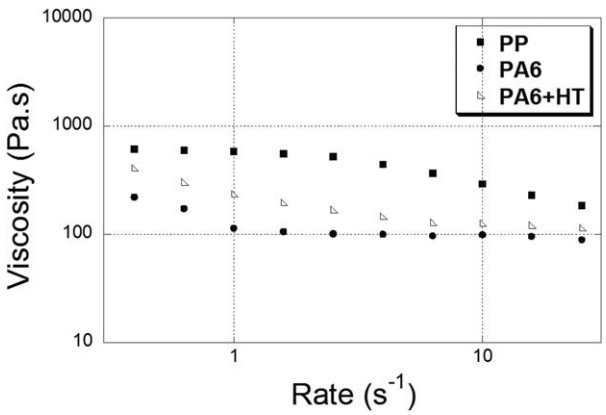

Figure 9. Steady state viscosity as a function of shear rate obtained for PP, PA6 matrix, and PA6/HT (4 wt %) nanocomposites at 240°C.

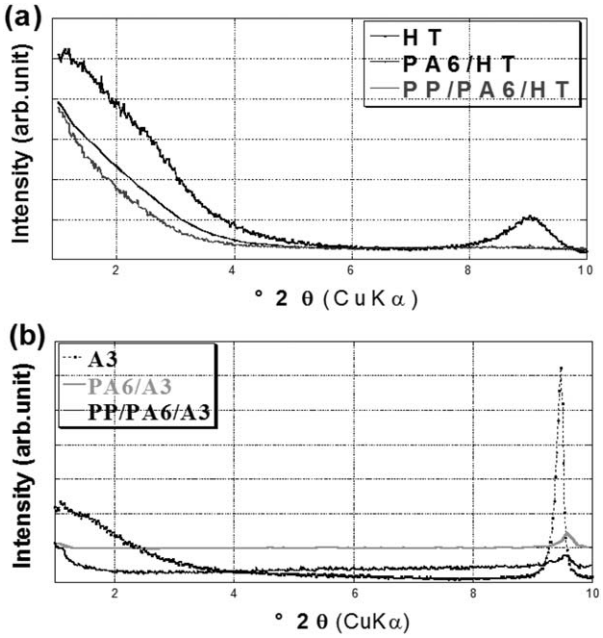

Figure 10. X-ray diffraction patterns of pure talc powder (—•—), PA6/talc binary nanocomposites (—), and PP/PA6/talc ternary blends (—).

talc layers within the PA6 nodules which confirms the TEM observations (Figure 4). Its highly polar character and its high ability to create strong acid-base interactions with the functional groups of polyamide 6 are the main reasons which explain the strong interfacial interactions generated between the synthetic talc and the polar matrix.[44]

In the opposite, the XRD spectra of natural talc filled PP/PA6 composites reveals almost no change concerning the peak position which indicates that the natural talc layers exist as aggregates within the nodules of PA6 since the natural talc lamellae have been found preferentially localized in the minor PA6 phase in the form of tactoids according to the previous TEM micrographs (Figure 4). Similar morphological structure was observed by Gahleitner et al. in the case of the unmodified montmorillonite filled PP/PA6 blends.[23] In fact, the authors highlighted that the natural montmorillonite (MMT) was strongly aggregated in PA6 phase and only a surface treatment of the clay by cationic exchange improved the dispersion of clay in PA6 phase.

Table IV. T_{onset} (Blend), T_{max}(PP), and T_{max}(PA6) of PP/PA6 Blend without Talc and PP/PA6 Blend Filled with Natural or Synthetic Talc

Sample	T_{onset} (°C)	T_{max} PP (°C)	T_{max} PA6 (°C)
PP/PA6	291.7	360.3	456.8
PP/PA6/HT	314.4	396.3	480.0
PP/PA6/A3	302.4	354.5	453.1

Thermal Stability of PP/PA6/Talc Blends

The degradation mechanisms of PP/PA6/talc blends have been studied by thermogravimetric analyses (TGA). Figure 11 shows the evolution of the weight loss as a function of temperature as well as the corresponding derivative curves of PP/PA6 blend without talc and with natural and synthetic talc. The onset temperature of degradation T_{onset} of PP/PA6/talc samples, the maximum decomposition temperature T_{max} of PP/PA6 blend are presented in Table IV.

PP/PA6 blends undergo firstly the degradation of polypropylene matrix followed by the degradation of the minority phase PA6. T_{onset} temperature of the unfilled blends was 291.7°C and the maximum decomposition temperature T_{max} of PP matrix and PA6 phase are 360.3 and 456.8°C, respectively. Unlike natural talc A3, the addition of synthetic talc in polymer blend has a positive effect on the thermal stability of PP/PA6 blends via the increase in their T_{onset} (+23°C) and especially a good improvement in T_{max} of the PP phase (+36°C) and in T_{max} of the PA6 component (+23°C). This result is consistent with what is found by Zhu et al.[45] in the case of MMT filled polypropylene/polystyrene nanocomposites. The authors suggested that the better the dispersion of clay in the dispersed phase (PS domains), the higher the thermal stability of the blends. Therefore, the presence of exfoliated silicate layers may be the main reason for the enhanced thermal stability of the compatibilized PP/PA6/HT hybrid.

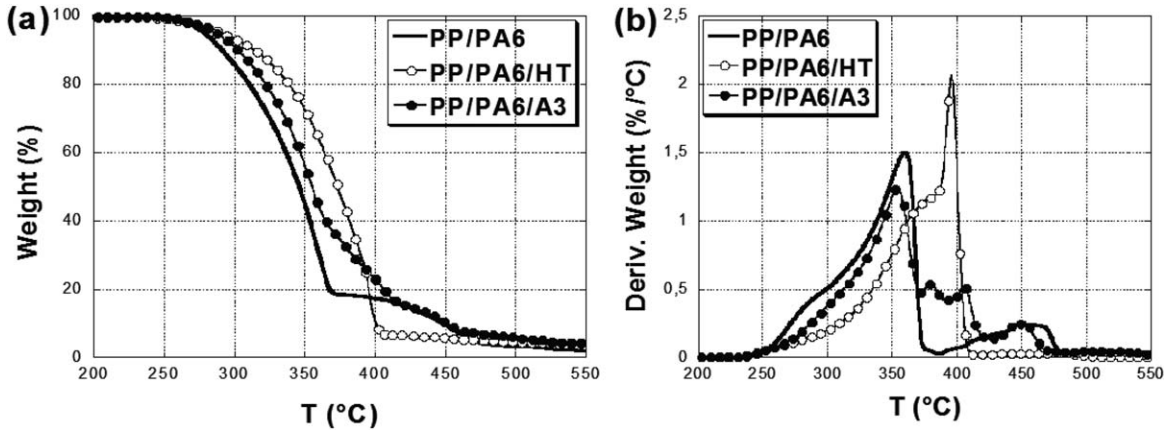

Figure 11. Evolution of weight loss as a function of temperature (TGA) and derivative of TGA curves (DTG) of PP/PA6 blend without talc and with natural and synthetic talc (heating rate: 20 K min^{-1}; air atmosphere).

Table V. Summary of Thermal Properties of Unfilled PP/PA6 and Talc Filled PP/PA6 Composites Estimated from DSC Studies

Echantillon	T_c(PP) (°C)	T_c PA6 (°C)	$t^{1/2}$ (PP) (min)	$t^{1/2}$ (PA6) (min)	T_m(PP) (°C)	T_m(PA6) (°C)	χ_c (PP) (%)	χ_c (PA6) (%)
PP/PA6	122.1	191.8	2.94	5.95	164.0	221.9	46.1	27.7
PP/PA6/A3	122.1	194.6	3.00	5.72	164.9	222.1	47.9	28.3
PP/PA6/HT	121.3	186.0	3.02	6.58	166.0	219.2	46.2	42.1

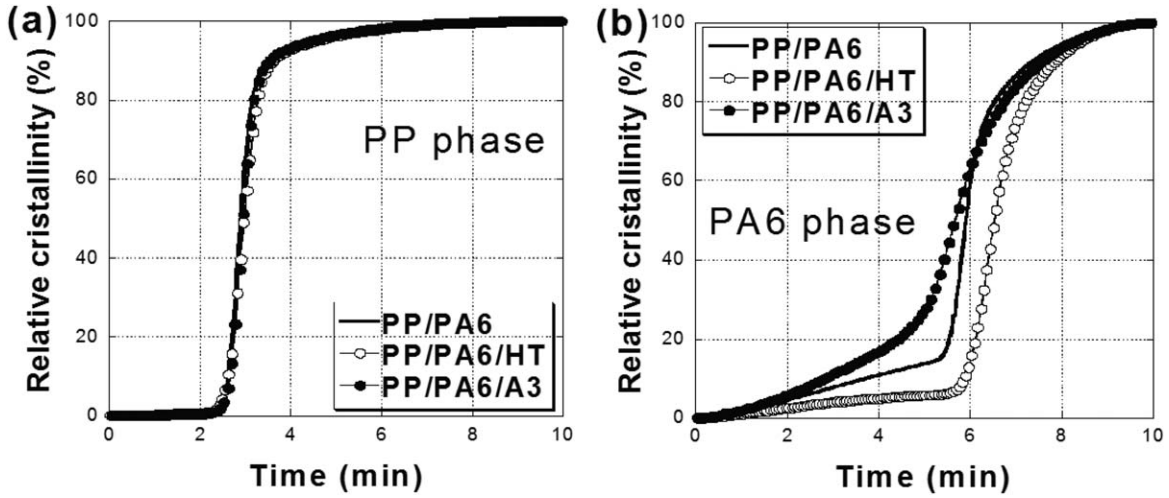

Figure 12. (a) Relative crystallinity as a function of time for the unfilled and talc filled PP/PA6/blends in (a) PP phase and (b) PA6 phase.

Effect of Talc Particles on Crystallization Behaviour of PP/PA6 Blends

Table V summarizes the melting and crystallization temperatures of unfilled PP/PA6 binary blends and PP/PA6/talc ternary blends. T_m, T_c designate the melting and crystallisation temperatures respectively, which are determined as the maximum of melting and crystallization peak from second heating and cooling respectively. $t^{1/2}$ represents the time corresponding to 50% of the relative crystallinity. χ_c (%) is the percent crystallinity of PP and PA6 phases in the blend.

Looking at the curve reporting the relative crystallinity as a function of time (Figure 12), the crystallization behaviour of PP matrix was almost unchanged regardless of the kind of talc introduced. The half crystallization time $t^{1/2}$ and the degree of crystallinity χ_c remained constant. However, the crystallisation profile of PA6 phase was influenced by the presence of talc. In fact, the natural talc A3 induces a nucleating effect with an acceleration of the rate of crystallization of PA6 and an increase in the crystallization temperature while the synthetic nanotalc HT induces an opposite effect where a slow-down of crystallization kinetics was observed. The degree of crystallinity of PA6 phase increases from χ_c of 27.7% in the unfilled PP/PA6 blends to χ_c of 42.1% in PP/PA6/HT samples. Similar trends was observed by Zhang et al.[46] which investigated the effect of multiwalled carbon nanotubes on the crystallisation behaviour of PA6/PP blends. The authors demonstrated that the addition of MWNTs decreased the crystallization rate of PA6 but increased the crystallinity of PA6 phase. According to the literature, this particular behaviour could be explained through the balance of the two opposite contributions of MWNTs. On the one hand, MWNTs acts as effective nucleating agent in PA6, whereas on the other hand, the same MWNTs have a confinement effect on spherulitic growth.[47] Similar trend was also observed by Cai and Wu[27] in the case of compatibilized PS/PA6/T_iO_2 blends. The presence of a higher number of synthetic silicate platelets evenly distributed at nanometer level inside the polyamide dispersed phase domains limits the growth of polyamide crystallites between the exfoliated layered silicates. This indicates that the compatibilisation process marginally slows the crystallization rate of the PA6 phase. Indeed, Xu[48] found in the case of PP/PBT blends compatibilized by adding side-chain liquid crystalline ionomer that the crystallization temperature of PBT component shifted to a lower temperature with the addition of SLCI. According to the author, the T_c of PBT component decreased on compatibilization, indicating that SLCI phase acted as a nucleating agent, and affected the crystallization rate of PBT.

Table VI. Mechanical Data from Tensile Tests Performed on Virgin PP/PA6 and PP/PA6/Talc Blends

Sample	PP/PA6	PP/PA6/A3	PP/PA6/HT
Young modulus (MPa)	1880	2140	2620
Standard deviation	16	199	294
Elongation at break (%)	17.2	37.2	9.0
Standard deviation	6.6	10.6	1.5
Yield stress (MPa)	28.8	37.8	31.6
Standard deviation	1.2	1.8	3.5

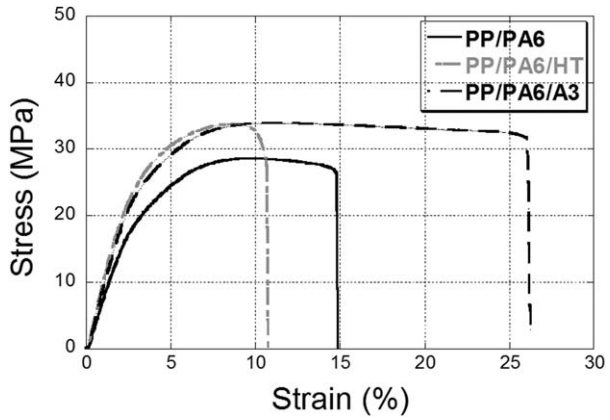

Figure 13. Stress–strain tensile curves for PP/PA6, PP/PA6/HT and PP/PA6/A3 blends.

Such a decrease in the crystallization temperature is known to enhance the compatibilization of immiscible mixtures.[49–51]

Mechanical Properties of PP/PA6/Talc Blends

The mechanical properties of the binary PP/PA6 and ternary PP/PA6/talc compounds with 4 wt % of talc are detailed in Table VI. Independently of talc used, an increase in Young's modulus was highlighted in talc filled ternary polymeric blends. However, the higher value in modulus is obtained for PP/PA6 blend filled with synthetic talc particles. In fact, one significant increase of 39.4% is observed (1880 MPa for the PP/PA6 blends and 2620 MPa with synthetic talc). The natural talc filled systems show only 14% of increase of Young's Modulus. This result can be explained by the poor dispersion of natural talc in the PA6 nodules.[44] However, compared with the neat blend, the standard deviation of Young modulus increases for the blends containing fillers probably due to the heterogeneity in the samples prepared on the mini-molding machine. It is interesting to note that the trend of the Young's modulus in the ternary PP/PA6/talc composites depending on the kind of talc used looks like PA6/talc systems previously studied[44] where the highest elastic modulus was measured on PA6/HT nanocomposites. This effect will be all the more important in the presence of large amount of nanotalc. As talc has an exclusive preference for the polar PA6 phase, the effective concentration of talc in PA6 will be five times more important (20 wt % against 4 wt %) which accentuates the reinforcing effect of talc on the blend.[20] compared with natural talc filled composites, the significant increase in the crystallinity of PA6 phase in the presence of synthetic nanofillers can also partly explains the higher stiffness of PP/PA6/HT nanocomposites. However, the elongation at break was found to be better (higher ductility) in the presence of PP/PA6/A3 systems than those prepared using the synthetic talc nanofillers (Figure 13). This result may look surprising as the morphology of this blend was composed of small PA6 nodules compared with PP/PA6/A3 blends containing much larger number of isolated microdomains. Similar behaviours were observed by Kusmono et al.[52] who showed that the addition of an organoclay (montmorillonite-octadecylamine) as a compatibilizer for PP/PA6 blend led to an increase in the stiffness of the blend but accompanied by a decrease in elongation at break due to the high exfoliation of sheets that restricts chain mobility. Using the same PP/PA6 (80/20) blends filled with nanosilica, Laoutid et al.[53] found that the nanofillers reduced the size of the dispersed domains but at the same time acted as stress concentrating particles which reduced the ductility of the PP matrix.

CONCLUSIONS

The incorporation of new nanoscale talc particles in immiscible PP/PA6 blends has resulted in remarkable improvements in the morphological structure evidenced by a dramatic reduction of the dispersed domain size revealed by SEM and TEM analysis.

The results show clearly that the final properties of blends are strongly linked to the hydrophilic/hydrophobic nature of talc investigated. The natural talc induces a nucleating effect on the PA6 dispersed phase as observed from an increase in the temperature of cristallization while the synthetic nanotalc gives an opposite effect where a slow-down of crystallization kinetics was observed. Such a decrease in the crystallization rate reflects the compatibilization effect induced by the addition of synthetic nanotalc. The strongest improvement in the thermal and mechanical properties of the materials was obtained again in the case of synthetic talc filled PP/PA6 nanocomposites. The new synthetic talc particles appear as promising fillers that can offer the "compatibilizer effect" for many immiscible polymer blends very frequently used in many industrial fields.

ACKNOWLEDGMENTS

This work was supported by financial funding from National Agency for Research (France) in the frame of the project "Nanotalc" ANR-09-MAPR-0017. The authors acknowledge Dr Annie Rivoire and Dr Ruben Verra from Claude Bernard University for their help in microscopy and XRD experiments, respectively.

REFERENCES

1. Maric, M.; Macosko, C. W. *Polym. Eng. Sci.*, **2001**, *41*, 118.
2. Lepers, J. C.; Favis, B. D.; Tabar, R. J. *J. Polym. Sci. Part B: Polym. Phys.*, **1997**, *35*, 2271.
3. Serpe, G.; Jarrin, J.; Dawans, F. *Polym. Eng. Sci.*, **1990**, *30*, 553.
4. Koning, C.; van Duin, M.; Pagnoulle, C.; Jerome, R. *Prog. Polym. Sci.* **1998**, *23*, 707.
5. Ide, F.; Hasegawa, A. *J. Appl. Polym. Sci.*, **1974**, *18*, 963.
6. Willis, J. M.; Favis, B. D. *Polym. Eng. Sci.*, **1988**, *28*, 1416.
7. Elias, L.; Fenouillot, F.; Majeste, J. C.; Martin, G.; Cassagnau, P. *J. Polym. Sci. Part B: Polym. Phys.*, **2008**, *46*, 1976.
8. Ray, S. S.; Bousmina, M. *Macromol. Rapid Commun.*, **2005**, *26*, 450.
9. Ray, S. S.; Pouliot, S.; Bousmina, M.; Utracki, L. A. *Polymer*, **2004**, *45*, 8403.
10. Dharaiya, D.; Jana, S. C. *Polymer*, **2005**, *46*, 10139.

11. Scaffaro, R.; Mistretta, M. C.; La Mantia, F. P. *Polym. Degrad. Stab.*, **2008**, *93*, 1267.
12. Yousfi, M.; Soulestin, J.; Vergnes, B.; Lacrampe, M.-F.; Krawczak, P. *J. Appl. Polym. Sci.*, **2013**, *128*, 2766.
13. Baudouin, A. C.; Devaux, J.; Bailly, C. *Polymer*, **2010**, *51*, 1341.
14. Garmabi, H.; Naficy, S. *J. Appl. Polym. Sci.*, **2007**, *106*, 3461.
15. Fenouillot, F.; Cassagnau, P.; Majeste, J. C. *Polymer* **2009**, *50*, 1333.
16. Tong, W.; Huang, Y. J.; Liu, C. L.; Chen, X. L.; Yang, Q.; Li, G. X. *Colloid Polym. Sci.*, **2010**, *288*, 753.
17. Benderly, D.; Siegmann, A.; Narkis, M. *J. Mater. Sci. Lett.*, *14*, 132 **1995**.
18. Huitric, J.; Ville, J.; Mederic, P.; Moan, M.; Aubry, T. *J. Rheol.*, **2009**, *53*, 1101.
19. Ville, J.; Mederic, P.; Huitric, J.; Aubry, T. *Polymer* **2012**, *53*, 1733.
20. Motamedi, P.; Bagheri, R. *Mater. Design*, **2010**, *31*, 1776.
21. Filippone, G.; Dintcheva, N. T.; Acierno, D.; La Mantia, F. P. *Polymer*, **2008**, *49*, 1312.
22. Ersoy, O. G.; Nugay, N. *Polym. Bull.* **2003**, *49*, 465.
23. Gahleitner, M.; Kretzschmar, B.; Pospiech, D.; Ingolic, E.; Reichelt, N.; Bernreitner, K. *J. Appl. Polym. Sci.*, **2006**, *100*, 283.
24. Ray, S. S.; Bousmina, M. *Macromol. Rapid Commun.*, **2005**, *26*, 1639.
25. Voulgaris, D.; Petridis, D. *Polymer*, **2002**, *43*, 2213.
26. Wang, Y.; Zhang, Q.; Fu, Q. *Macromol. Rapid Commun.*, **2003**, *24*, 231.
27. Cai, X.; Wu, G. *J. Macromol. Sci. Part B: Phys.*, **2013**, *53*, 347.
28. Le Roux, C.; Martin, F.; Micoud, P.; Dumas, A. *Int. Pat. WO,004,979*, **2013**.
29. Dumas, A.; Martin, F.; Le Roux, C.; Micoud, P.; Petit, S.; Ferrage, E.; Brendlé, J.; Grauby, O.; Greenhil-Hooper, M. *Phys. Chem. Miner.* **2013**, *40*, 361.
30. Owens, D. K.; Wendt, R. C. *J. Appl. Polym. Sci.*, **1969**, *13*, 1741.
31. Clark, E. J.; Hoffman, J. D. *Macromolecules*, **1984**, *17*, 878.
32. Cartledge, H. C. Y.; Baillie, C. A. *J. Mater. Sci.*, **1999**, *34*, 5099.
33. Schrader, M. E.; Yariv, S. *J. Colloid Interface Sci.*, **1990**, *136*, 85.
34. Lobato, E. *PhD Thesis; Virginia Tech, USA*, **2004**.
35. Girifalco, L. A.; Good, R. J. *J. Phys. Chem.*, **1957**, *61*, 904.
36. Zhu, Y.; Ma, H. -Y.; Tong, L. -F.; Fang, Z. -P. *J. Zhejiang Univ. Sci. A*, **2008**, *9*, 1614.
37. Cai, X. X.; Li, B. P.; Pan, Y.; Wu, G. Z. *Polymer*, **2012**, *53*, 259.
38. Sumita, M.; Sakata, K.; Asai, S.; Miyasaka, K.; Nakagawa, H. *Polym. Bull.*, **1991**, *25*, 265.
39. Lagaly, G.; Reese, M.; Abend, S. *Appl. Clay Sci.*, **1999**, *14*, 83.
40. Ou, B.; Li, D.; Liu, Y. *Compos. Sci. Technol.* **2009**, *69*, 421.
41. Elias, L.; Fenouillot, F.; Majeste, J. C.; Alcouffe, P.; Cassagnau, P. *Polymer*, **2008**, *49*, 4378.
42. Wu, S. H., *Polym. Eng. Sci.*, **1987**, *27*, 335.
43. Si, M.; Araki, T.; Ade, H.; Kilcoyne, A. L. D.; Fisher, R.; Sokolov, J. C.; Rafailovich, M. H. *Macromolecules*, **2006**, *39*, 4793.
44. Yousfi, M.; Livi, S.; Dumas, A.; Le Roux, C.; Crépin-Leblond, J.; Greenhill-Hooper, M.; Duchet-Rumeau, J. *J. Colloid Interface Sci.*, **2013**, *403*, 29.
45. Zhu, Y.; Ma, H. -Y.; Tong, L. -F.; Fang, Z. -P. *Chin. J. Polym. Sci.* **2008**, *26*, 783.
46. Zhang, L.; Wan, C.; Zhang, Y. *Polym. Eng. Sci.*, **2009**, *49*, 1909.
47. Valentini, L.; Biagiotti, J.; Kenny, J. M.; Manchado, M. A. L. *J. Appl. Polym. Sci.* **2003**, *89*, 2657.
48. Xu, X. -Y. *Chem. Res. Chin. Univer.* **2011**, *27*, 140.
49. Sun, Y. J.; Hu, G. H.; Lambla, M.; Kotlar, H. K. *Polymer*, **1996**, *37*, 4119.
50. Ahn, T. O.; Lee, S.; Jeong, H. M.; Lee, S. W. *Polymer*, **1996**, *37*, 3559.
51. Zhang, B. -Y.; Sun, Q. -J.; Li, Q. -Y.; Wang, Y. *J. Appl. Polym. Sci.*, **2006**, *102*, 4712.
52. Kusmono; Ishak, Z. A. M.; Chow, W. S.; Takeichi, T.; Rochmadi, *Eur. Polym. J.*, **2008**, *44*, 1023.
53. Laoutid, F.; Estrada, E.; Michell, R. M.; Bonnaud, L.; Mueller, A. J.; Dubois, P., *Polymer*, **2013**, *54*, 3982.